HiSST: 2nd International Conference on
High-Speed Vehicle Science & Technology
11-15 September 2022, Bruges, Belgium

Hypersonic aerodynamic predictions for arbitrary geometries using ANTARES

Thomas Durbin[1], *Guillaume Grossir*[2] *and Olivier Chazot*[3]

Abstract

Aerodynamic predictions in the hypersonic regime may be obtained to a good degree of accuracy using the Newtonian theory. The present paper describes the ANTARES code (short for Application of Newtonian Theory for ARbitrary Entry Shapes) which has been developed at the von Karman Institute for Fluid Dynamics for such predictions on 3-dimensional arbitrary geometries. Wall pressure distributions, aerodynamic forces and moments as well as their corresponding coefficients can be predicted efficiently. Results are presented for several academic geometries and for real configurations (Apollo, the Space Shuttle and a hemispherical space debris geometry). Predictions are validated against analytical results, wind tunnel data, flight measurements, and/or numerical values. Special features of the code are briefly described, including shadowing effects and center of pressure computation capabilities.

Keywords: *hypersonic, aerodynamics, modified Newtonian theory, forces, moments, pressure distributions, 3D, center of pressure*

Nomenclature

Latin

C_p	Pressure coefficient, -
C_D	Drag coefficient, -
C_L	Lift coefficient, -
C_M	Pitching moment coefficient, -
$C_{p,\text{max}}$	Stagnation point pressure coefficient, -
l	length, m
M	Mach number, -
p	Pressure, Pa
R_I	Rotation matrix from body to inertial reference frame
R	radius, m
S	Surface, m^2
u	Flow velocity, m/s
x, y, z	Cartesian coordinates, m

Greek

α	Angle of attack, degrees
β	Angle from stagnation point, degrees
γ	Specific heat ratio, -
θ	Inclination of a surface with the free-stream velocity vector, degrees
θ	Pitch angle, degrees
ρ	Flow density, kg/m^3
ϕ	Roll angle, degrees
ψ	Yaw angle, degrees

Subscripts

∞	free-stream value
B	base
cp	center of pressure
C.G.	at the center of gravity
n	normal component
N	nose
ref	reference
w	at the wall

[1] *Graduate student, von Karman Institute for Fluid Dynamics, Rhode-Saint-Genèse, Belgium*
[2] *Senior Research Engineer, von Karman Institute for Fluid Dynamics, Rhode-Saint-Genèse, Belgium, grossir@vki.ac.be*
[3] *Professor and Head of Department, von Karman Institute for Fluid Dynamics, Rhode-Saint-Genèse, Belgium, chazot@vki.ac.be*

1. Introduction

1.1. Motivation

Trajectory predictions for reentry vehicles or space debris using 3 to 6 degrees of freedom codes require accurate aerodynamic databases covering a wide range of attitudes. Establishing such databases using either experimental or numerical approaches is usually not affordable from an economical point of view. Theoretical predictions based on the Newtonian theory can be used as an alternative, especially during the preliminary design phase, for a fraction of the original cost.

1.2. Objectives

The main objective of the present work is to efficiently implement the modified Newtonian theory for arbitrary 3-dimensional geometries and to validate the corresponding predictions (pressure distributions, aerodynamic forces/moments and their corresponding coefficients, center of pressure...) against different sources available from the literature.

1.3. Outline

Some background about the Newtonian theory is briefly described in §2. The ANTARES code (short for Application of Newtonian Theory for ARbitrary Entry Shapes) that has been developed at the VKI in order to predict accurate aerodynamic coefficients for arbitrary geometries in the hypersonic regime is then presented in §3. It is followed in §4 by a description of several test cases where the aerodynamic predictions of academic geometries and real flight configurations are compared with analytical, experimental and numerical results.

2. Newtonian flow model

Isaac Newton introduced in his famous 1687 work "Principia", a fluid dynamic theory that aimed to estimate the forces acting on an inclined surface with respect to the incoming flow. This inviscid theory assumes that the flow is composed of a rectilinear stream of particles which are not deviated until they reach a surface, and which upon hitting this surface inclined at an angle θ to the stream, would transfer all their momentum normal to that surface, but preserve their tangential momentum, as illustrated in Fig. 1. While the Newtonian theory was found to be conceptually inaccurate for most flow regimes, it has an important application today in hypersonic flows, for which it turned out to be a good approximation [1] when pressure forces dominate the friction ones, and provided that $M_\infty\theta \gg 1$ (thin shock layer assumption).

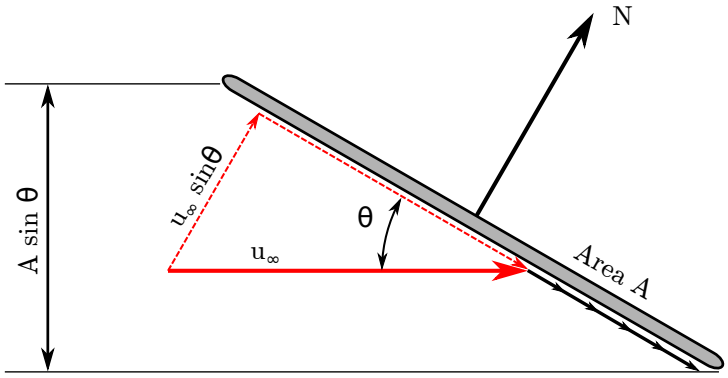

Fig 1. Schematic used for the derivation of Newton's sine-squared law [2].

Following Newton's hypothesis, the wall pressure p_w along the inclined surface illustrated in Fig. 1 can be

expressed using the momentum equation for a streamtube normal to the inclined surface (eq. 1).

$$p_w = p_\infty + \rho_\infty u_{\infty,n}^2 \tag{1}$$

$$p_w = p_\infty + \rho_\infty \left(u_\infty \sin\theta\right)^2 \tag{2}$$

Rearranging the different terms leads to:

$$\frac{p_w - p_\infty}{\frac{1}{2}\rho_\infty u_{\infty,n}^2} = 2\sin^2\theta \tag{3}$$

which corresponds to the expression of a local pressure coefficient:

$$C_p = 2\sin^2\theta \tag{4}$$

The Newtonian theory is characterized by this single equation that is known as Newton's sine-squared law, with a stagnation point coefficient equal to 2. A modification to this law (eq. 5) was first proposed in 1955 by Lees [3] who remarked that the stagnation point coefficient was smaller than 2, even for large Mach numbers. This is now widely known as the modified Newtonian law, where the local pressure coefficient C_p is expressed as:

$$C_p = C_{p,\text{max}} \sin^2\theta. \tag{5}$$

where $C_{p,\text{max}}$ corresponds to the stagnation point coefficient that exists at the stagnation point downstream of a normal shock. This value is typically estimated from eq. 6 for blunt bodies. The Newtonian value $C_p = 2$ is retrieved in the limit of $M_\infty \to \infty$ and $\gamma \to 1$.

$$C_{p,\text{max}} = \frac{2}{\gamma M_\infty^2}\left(\left[\frac{(\gamma+1)^2 M_\infty^2}{4\gamma M_\infty^2 - 2(\gamma-1)}\right]^{\frac{\gamma}{\gamma-1}}\left[\frac{1-\gamma+2\gamma M_\infty^2}{\gamma+1}\right] - 1\right) \tag{6}$$

All surfaces not exposed directly to the incoming flow are assumed to be in a shadow region, and are characterized by a local pressure coefficient $C_p = 0$.

Although, there are some limitations to the applicability of such a model in presence of shock interactions for instance, it remains attractive for a quick estimation of the pressure distribution along hypersonic bodies. The surface of these vehicles can be discretized into small planar surface elements, along which the local pressure coefficient can be evaluated using eq. 5. The corresponding pressure acting on each element, and the associated forces follow from this pressure coefficient. Upon integration of these quantities all over the object, the global aerodynamic forces and moments acting on the vehicle can be obtained, together with other quantities of interest such as the center of pressure. This has been used extensively for engineering purposes [4–7].

3. The ANTARES code

The main features of the ANTARES code (short for Application of Newtonian Theory for ARbitrary Entry Shapes) are described next.

Reference free-stream flow quantities: Free-stream flow properties are defined at first: the specific heat ratio γ of the gas, the free-stream Mach number M_∞, and the free-stream static pressure p_∞. The former two quantities enter in the expression of the maximum stagnation point pressure coefficient (eq. 6). The latter is useful only if the absolute magnitude of the aerodynamic forces needs to be determined, otherwise it can be selected arbitrarily as it does not influence the aerodynamics coefficients (non-dimensionalized by the reference dynamic pressure $\frac{\gamma}{2}p_\infty M^2$).

3D geometry, object attitude: The code then requires a surface mesh that represents the geometry. Both binary STL and ASCII STL formats, obtained from usual CAD softwares, are convenient since they consist of an unstructured triangular mesh that is defined by a series of faces and vertices. The attitude of the vehicle with respect to the incoming flow is defined by Tait–Bryan angles (yaw ψ, pitch θ, and roll ϕ) following the standard aerospace convention. The rotation from the body frame to the inertial reference frame is achieved using eq. 7. Its transpose serves for the opposite transformation.

$$R_{\mathrm{I}} = R_\psi R_\theta R_\phi = \begin{bmatrix} c_\psi c_\theta & c_\psi s_\theta s_\phi - s_\psi c_\phi & c_\psi s_\theta c_\phi + s_\psi s_\phi \\ s_\psi c_\theta & s_\psi s_\theta s_\phi + c_\psi c_\phi & s_\psi s_\theta c_\phi - c_\psi s_\phi \\ -s_\theta & c_\theta s_\phi & c_\theta c_\phi \end{bmatrix} \tag{7}$$

Newtonian impact model: The normal vectors to each surface element composing the object are determined next. This enables to compute the orientation of each surface with respect to the incoming flow. If the corresponding angle $\theta < 90\,^\circ$, then the pressure coefficient along this surface element is inferred from eq. 5. Otherwise, the surface lays in the shadow of the object and the local pressure coefficient is assumed to be equal to 0 (i.e. the local pressure is equal to the free-stream static pressure). Rather than performing these computations for each surface element in a sequential manner using loops, ANTARES heavily relies on the vectorization capabilities offered by Matlab for improved performances.

Shadowed surfaces: The pressure coefficient along surfaces oriented towards the incoming flow but protected partially or completely by upstream surfaces do not follow eq. 5: this is usually referred to as shadowing effects. It is treated in ANTARES similarly to the approach described by [8] using a projection method. The local pressure coefficient acting on that surface is then either set to 0 (when it is completely shadowed by upstream elements) or taken as the original pressure coefficient corrected by the ratio of the exposed surface to the surface area.

Local pressure, aerodynamics forces and moments: Quantities of interest follow directly from the definition of the pressure coefficient, such as the local pressure acting on each elementary surface, and the corresponding force that can be decomposed into three components along the body and/or inertial axes. The moments induced by these forces around the center of gravity (or any other arbitrary points) is then evaluated.

The aerodynamic loads applied onto the body are obtained by integrating the forces acting on all surfaces. This yields the lift, drag and side forces (in the inertial frame), and the axial, normal and side forces (in the body frame). The moments around the three reference axes are obtained similarly by summing contributions from all surface elements and can be expressed either in the inertial system or in the body one. The corresponding aerodynamic coefficients follow from the reference dynamic pressure, a reference surface, and a reference length for the moments.

Additional features: ANTARES further allows to extract pressure profiles along arbitrary cross-sections of the geometry, displays the location of the stagnation point, predicts the center of pressure from which the static margin of the vehicle can be inferred... Several examples are presented in §4 and demonstrate the accuracy and the performances of the ANTARES code.

4. Results

4.1. Academic geometries

Academic geometries such as flat plates, spheres or cylinders all have an analytic solution for their aerodynamic coefficients. Using the ANTARES code for these geometries is obviously not required but it still serves to check the implementation of the Newtonian model in the code.

4.1.1. Flat plate

The lift and drag coefficients of a flat plate as a function of the angle of attack α can be expressed theoretically by eqs. 8 and 9 [1], assuming here a stagnation point pressure coefficient equal to 2, as

for the original Newtonian model. Predictions from the ANTARES code using the same assumption are shown in Fig. 2 and indeed overlap with the theoretical solution.

$$C_L = 2\sin^2(\alpha)\cos(\alpha) \tag{8}$$

$$C_D = 2\sin^3(\alpha) \tag{9}$$

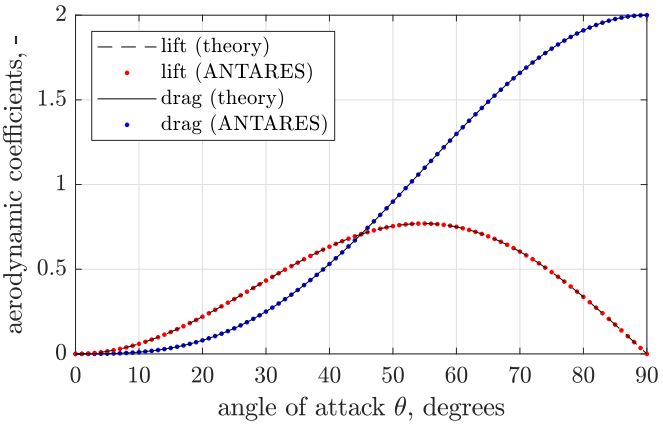

Fig 2. Drag and lift coefficients for a flat plate at different angles of attack. Comparison between analytical results and ANTARES predictions.

4.1.2. Sphere

A spherical case is considered next, with different CAD models featuring an increasing resolution of the surface (as illustrated in Fig. 3a to 3f). The local pressure coefficient determined from eq. 5 is plotted as a function of the angle β (away from the stagnation point) in Fig. 3g.

The corresponding drag coefficient obtained from the integration of the local forces over the whole object is then plotted in Fig. 3h. Results from the convergence study show that using a coarse mesh with as few as 180 elements for the whole sphere yields a drag coefficient that is already within 1.7% of the analytical value ($C_D = 1$, if $C_{p,\text{max}} = 2$ [9]). The computational time for the sphere with a surface mesh approaching half a million surface elements remains below 1 second thanks to the efficient implementation within ANTARES.

4.1.3. Cones

The hypersonic aerodynamics of sharp cones have been derived analytically [1] including flight configurations where the angle of attack of the object is exceeding their opening half-angles (in which case a part of the surface of the cone is shadowed from the incoming flow). Similar analytical results were also derived for blunt cones at small angles of attack. A few aerodynamic results for sharp and blunt cones are reported in Fig. 4, including comparison against experimental data [10] and predictions from the ANTARES code. The reference surface is taken as the base area of the cone ($S_{\text{ref}} = \pi R^2$), and the reference length is the base diameter.

The agreement among the different approaches is mostly excellent. ANTARES predictions match analytical predictions from 0 to 90° angle of attack (beyond this value, the theory does not account for the fact that the base of the cone becomes exposed to the incoming flow). Results presented in Fig. 4d for the pitching moment coefficient also serve to validate the computation of moments within the ANTARES code. The overall agreement with reference experimental data is also remarkable regardless of the nosetip bluntness that is considered.

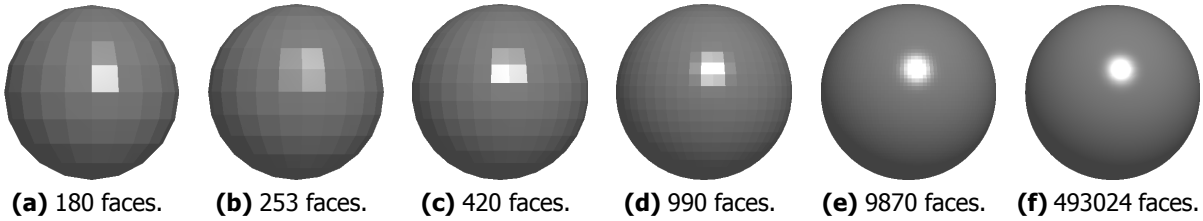

(a) 180 faces. **(b)** 253 faces. **(c)** 420 faces. **(d)** 990 faces. **(e)** 9870 faces. **(f)** 493024 faces.

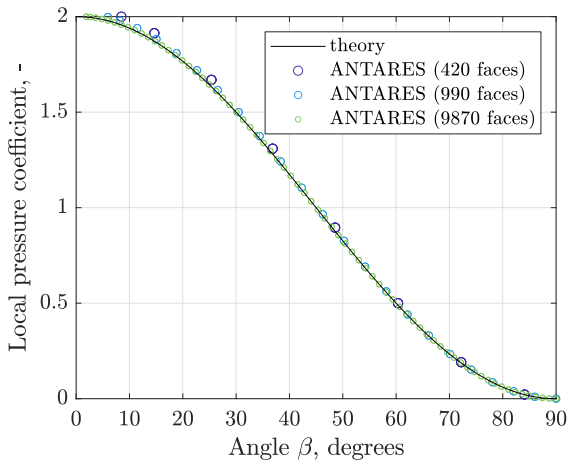

(g) Pressure distribution at the center of the face.

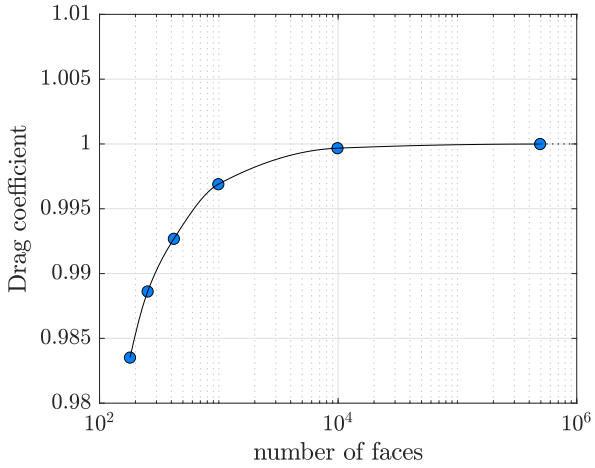

(h) Drag coefficient.

Fig 3. Mesh dependence study for a spherical body.

It is important to note that on such slender geometries the relative contribution of the skin friction on the overall aerodynamic forces increases. This is not accounted for by the Newtonian theory which accounts only for the pressure contribution, and also neglects contributions from the base pressure [11]. It is important to note that the Newtonian predictions for the conical geometries reported here were all obtained assuming a stagnation point pressure coefficient $C_{p_{max}} = 2$, i.e., as with the original Newtonian formulation.

Even though an analytical solution can be obtained for the aerodynamics of conical geometries [1], it requires rather lengthy derivations, and this is where a numerical integration of the forces acting on the geometry starts to prove useful.

The forces and moments acting on the geometry being known, they can be used to determine the location of the center of pressure. An example is given in Fig. 5 for four sharp cones (half-angle equal to 5, 7, 10, and 20°) while increasing their angle of attack. The axial location of the center of pressure is located at two third of the body length in all cases, regardless of the angle of attack, in agreement with analytical results [6]. The radial location of the center of pressure y_{cp} matches the analytical results reported in [9] as long as the angle of attack α remains smaller than the opening angle of the cone. The Newtonian results again prove useful to extend the determination of the center of pressure to cases for large angles of attack, where analytical results do not apply. The location of this point with respect to the center of gravity conditions the static stability of the vehicle. It can be determined easily with ANTARES.

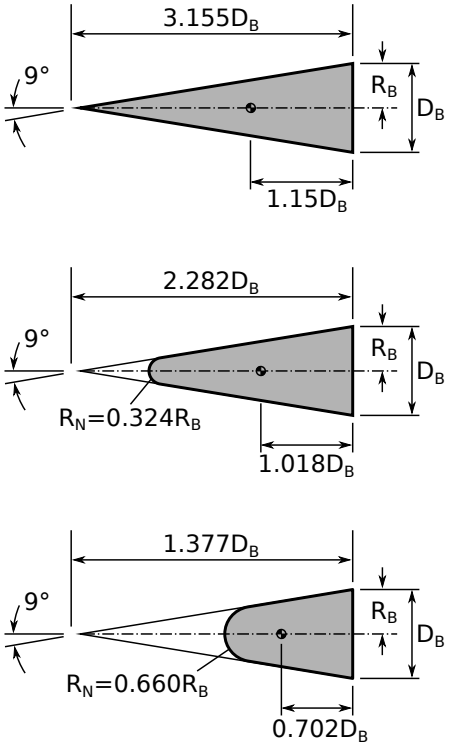

(a) Conical geometries considered [10].

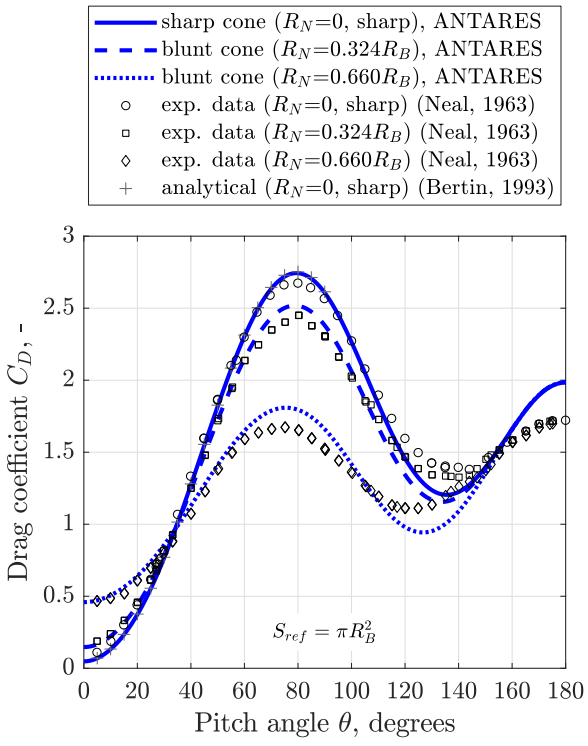

(b) Drag coefficient.

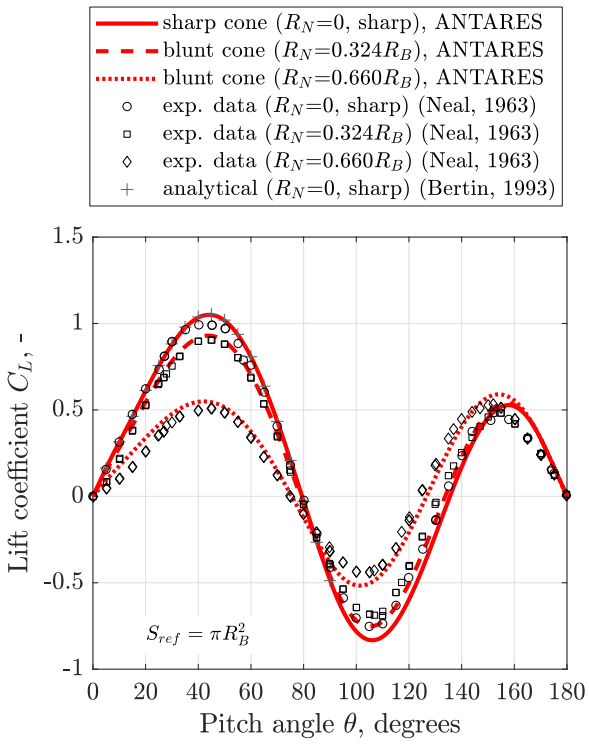

(c) Lift coefficient.

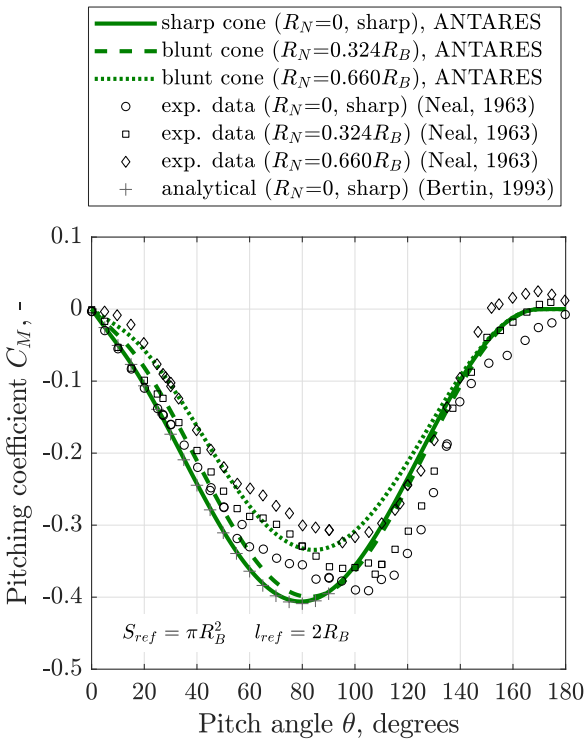

(d) Pitching moment coefficient are computed around a point located at $2.3R_B$, $2.036R_B$ and $1.404R_B$ from the base for different nosetip bluntness varying between $0 \leq \frac{R_N}{R_B} \leq 0.66$, respectively.

Fig 4. Aerodynamic coefficients for a sharp and blunt cones. Experimental data obtained for Mach 6.77.

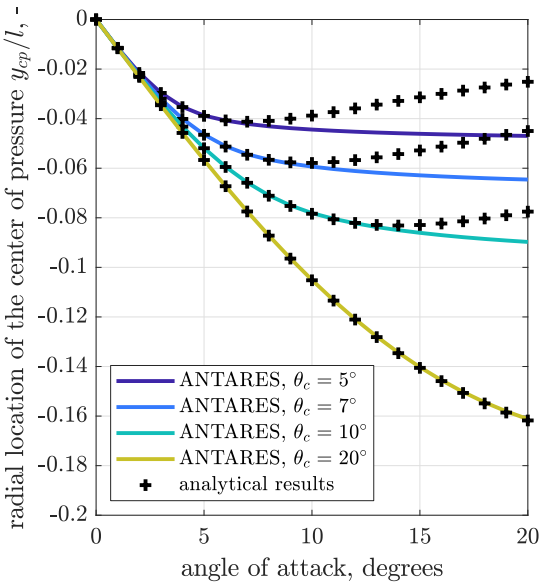

Fig 5. Radial location of the center of pressure for sharp cones as predicted by the Newtonian theory compared with analytical results. The axial location is located at $x_{cp} = \frac{2}{3}l$.

4.2. Real configurations: reentry vehicles and space debris

Predictions from the ANTARES code have been shown in §4.1 to match analytical results over simple academic geometries. Such a code is obviously not limited to simple geometries and its interest actually resides in the possibility to apply it in the same way to more complex geometries as described hereafter for which there exists no analytical solutions.

4.2.1. Apollo

Aerodynamic predictions for the Apollo Command Module are obtained using the geometry presented in Fig. 6. The reference area is taken as the frontal surface of the capsule and the reference length corresponds to its diameter.

The pressure distribution along the Apollo command module's pitch plane centerline for an angle of attack of 25° is illustrated in Fig. 7. Predictions are in excellent agreement with data from flight AS-201 [12].

The aerodynamic coefficients of the vehicle (lift, drag and pitching moment around its center of gravity) are obtained by integrating the pressure over the whole object and the corresponding results are reported in Figs. 8a to 8d. Comparison against experimental data demonstrate again the accuracy of the modified Newtonian approach for this geometry over a wide range of attitudes.

4.2.2. Space Shuttle

The pressure distribution along the Space Shuttle[1] can be determined using the same approach. This vehicle used to reenter the Earth with large angles of attack, exposing its blunt underbody to the incoming flow and shadowing at the same time other surfaces (vertical fin, engine pods...). This can be accounted for in ANTARES, as illustrated in Fig. 9 with a drag coefficient reducing by as much as 9.5% at $\alpha = 40\,°$ when shadowing effects are accounted for. In this particular case, the engine bays are protected from the incoming flow by the wings.

[1]CAD model is from https://grabcad.com/library/space-shuttle–1.

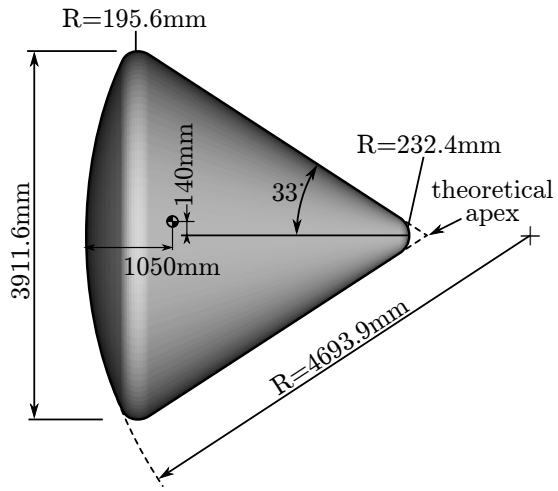

Fig 6. Dimensions of the Apollo vehicle

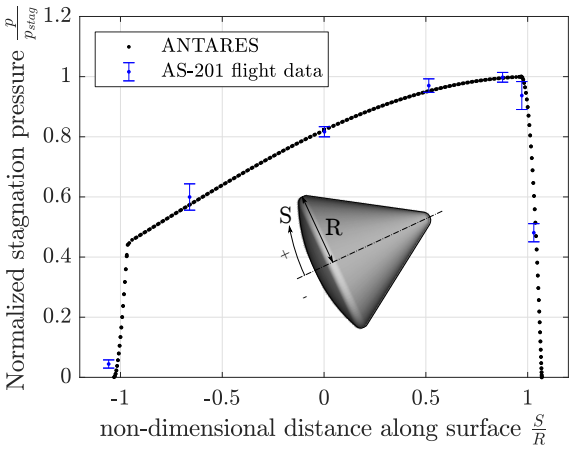

Fig 7. Comparison between ANTARES predictions and flight data [12] for the normalized pressure along the Apollo command module's pitch plane centerline for an angle of attack of 25°.

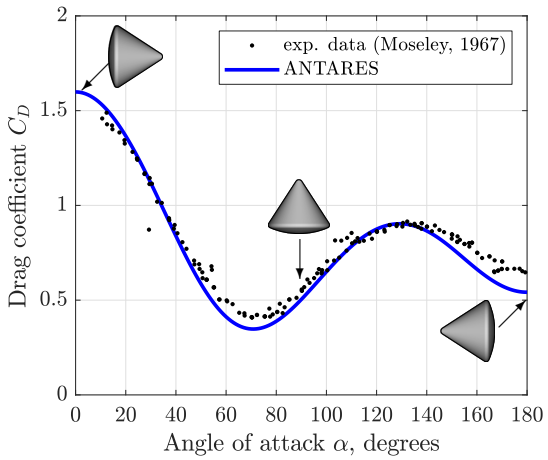

(a) Drag coefficient C_D.

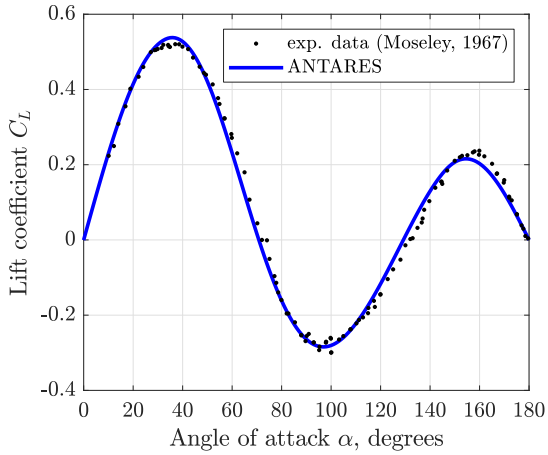

(b) Lift coefficient C_L.

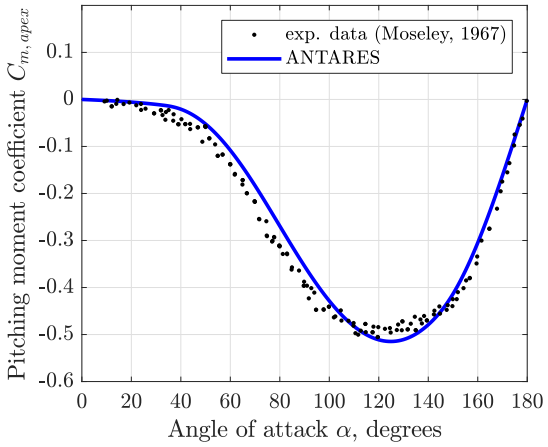

(c) Pitching moment coef. $C_{my,\text{apex}}$.

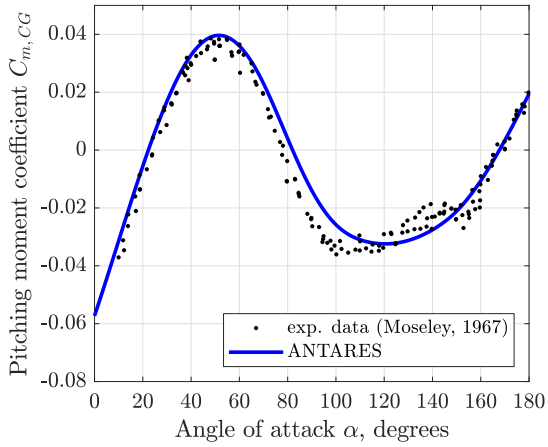

(d) Pitching moment coef. $C_{my,\text{C.G.}}$.

Fig 8. Aerodynamic coefficients of the Apollo Command Module obtained from a Newtonian model compared against experimental data extracted from [13].

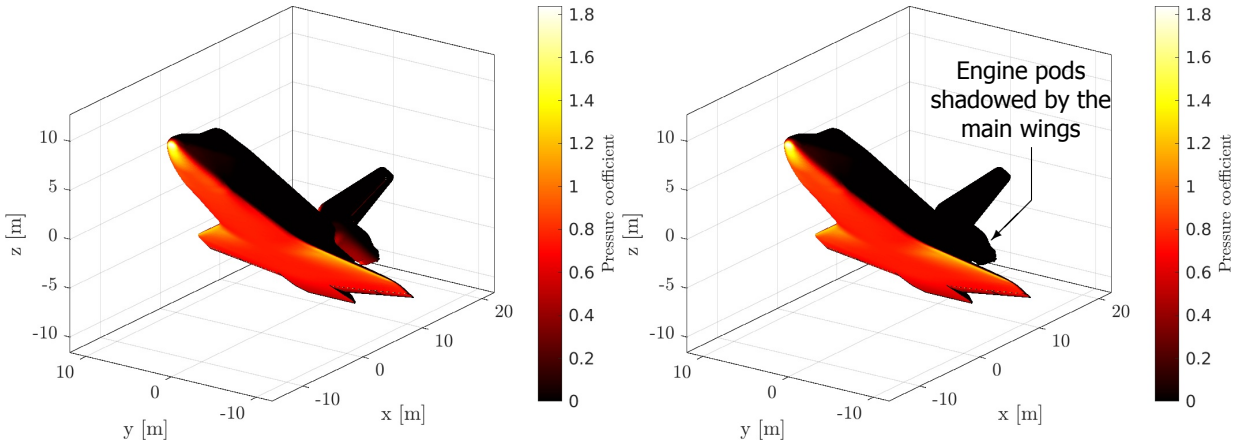

(a) Neglecting shadowing effects ($C_D = 0.8167$). **(b)** Accounting for shadowing effects ($C_D = 0.7460$).

Fig 9. Comparison between modified Newtonian pressure predictions on the Space Shuttle for an angle of attack of 40° illustrating the influence of shadowing effects on the aft geometry of the orbiter.

4.2.3. Space debris

The aerodynamics of space debris may also be predicted by ANTARES. An example for an hemispherical shell issuing from a split propellant tank is considered in Fig. 10. Shadowing effects also take place on this geometry (as illustrated in Fig. 10a) but the best match with experimental data is actually obtained with the assumption that the geometry is filled instead of being concave. This is demonstrated in Fig. 10b where the ANTARES predictions accurately match the experimental and numerical lift coefficient over the complete range of attitudes. The agreement is not as good for the drag coefficient (Fig. 10c) when the cavity is filled, but still better follows the reference trends when compared to the hollow case. Experimental and numerical data are extracted from [14, 15] where further analysis of the aerodynamics of this space debris and an annular one are reported.

5. Summary

It is well established that a modified Newtonian flow model can predict the aerodynamics of hypersonic vehicles in the continuum regime to a good degree of accuracy. This model has been implemented within the ANTARES code for arbitrary 3D geometries. Predictions have been validated against reference theoretical data (for simple shapes for which an analytic solution can be derived), and also against experimental and numerical data for more complex geometries (real entry vehicles, space debris...).

Overall, the ANTARES code enables to determine pressure distributions, forces/moments and the corresponding coefficients for 3-dimensional hypersonic geometries for a low computational cost. Shadowing effects can also be accounted for and are shown to improve the quality of the predictions.

The limitations of the underlying theory remain associated with cases presenting shock impingement with the surfaces or compressions through multiple shock waves [1]. For the specific case of concave surfaces, an example with a hollow hemisphere shows that it is aerodynamic coefficients can be predicted with a better accuracy assuming that the object is filled instead of being concave. Although it might not apply to all concave geometries with the same accuracy, it proves to be more relevant for the aerodynamics of a common type of space debris.

ANTARES predictions can typically be tabulated and fed into reentry trajectory codes for improved reentry trajectory predictions. Extension of the code towards the rarefied flow regime would further enlarge the field of application of this tool.

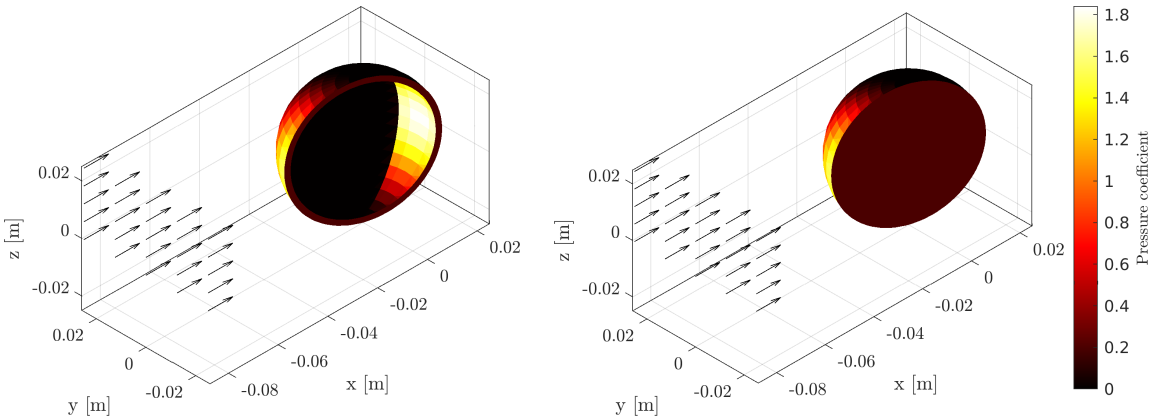

(a) Hemispherical geometry treated with two different approaches (left: hollow model, accounting for shadowing effects; right: cavity is filled to yield a plain model) leading to a major influence on their aerodynamics.

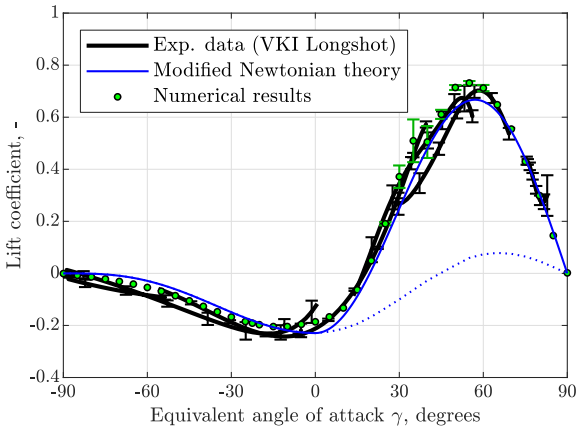

(b) Lift coefficient. Newtonian predictions are indicated for a hollow hemisphere (····) and for a filled one (——).

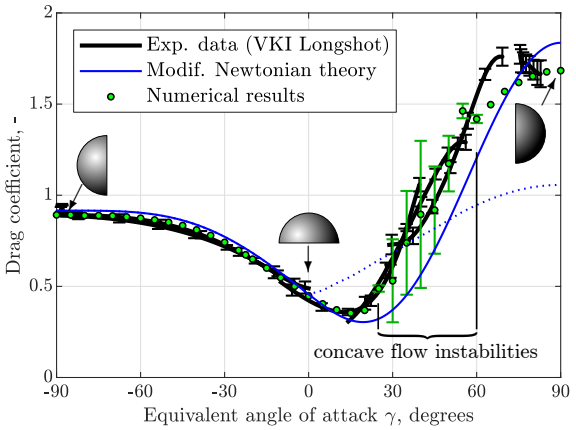

(c) Drag coefficient. Newtonian predictions are indicated for a hollow hemisphere (····) and for a filled one (——).

Fig 10. Application of the Newtonian theory to a hemispherical space debris.

References

[1] J. J. Bertin. *Hypersonic aerothermodynamics*. AIAA, 1994.

[2] J. D. Anderson. *Hypersonic and High Temperature Gas Dynamics*. American Institute of Aeronautics and Astronautics, second edition, 2006.

[3] L. Lees. Hypersonic flow. In *5th International Aeronautical conference*, pages 241–276, Los Angeles, 1955. Institute of Aeronautical Sciences.

[4] W. R. Wells and W. O. Armstrong. Tables of aerodynamic coefficients obtained from developped newtonian expressions for complete and partial conic and spheric bodies at combined angles of attack and sideslip with some comparisons with hypersonic experimental data. Technical Report TR R-127, NASA Langley Research Center, 1962.

[5] E. L. Clark and L. L. Trimmer. Equations and charts for the evaluation of the hypersonic aerodynamic characteristics of lifting configurations by the newtonian theory. Technical Report AEDC-TR-64-25, Arnold Engineering Development Center, March 1964.

[6] F. Garcia, Jr. Comment on the location of the center of pressure of a right circular cone using newtonian impact theory. *AIAA Journal*, 4(6):1150–1151, June 1966.

[7] M. L. Rasmussen. Stability derivatives for hypersonic waveriders according to newtonian theory. In *20th Atmospheric Flight Mechanics Conference*, number AIAA paper 1995-3492, August 1995.

[8] Y. Prevereaud. *Contribution à la modélisation de la rentrée atmosphérique des débris spatiaux*. PhD thesis, Université de Toulouse, June 2014.

[9] J. J. Bertin and R. M. Cummings. *Aerodynamics for engineers*. Pearson, 6th edition, 2014.

[10] L. Neal, Jr. Aerodynamic characteristics at a Mach number of 6.77 of a 9° cone configuration, with and without spherical afterbodies, at angles of attack up to 180° with various degrees of nose blunting. Technical Report NASA TN D-1606, Langley Research Center, March 1963.

[11] G. S. Pick. Base pressure distribution of a cone at hypersonic speeds. *AIAA Journal*, 10(12):1685–1686, December 1972.

[12] D. B. Lee. Apollo experience report - Aerothermodynamics evaluation. Technical Report NASA TN D-6843, NASA, June 1972.

[13] W. C. Moseley, Jr, R. H. Moore, Jr, and J. E. Hughes. Stability characteristics of the Apollo Command Module. Technical Report NASA TN D-3890, National Aeronautics and Space Administration, March 1967.

[14] G. Grossir, D. Puorto, Z. Ilich, S. Paris, O. Chazot, S. Rumeau, M. Spel, and J. Annaloro. Aerodynamic characterization of space debris in the VKI Longshot hypersonic tunnel using a free-flight measurement technique. In *International Conference on Flight vehicles, Aerothermodynamics and Re-entry Missions and Engineering (FAR)*, September-October 2019.

[15] J. Annaloro, S. Galera, C. Thiebaut, M. Spel, P. Van Hauwaert, G. Grossir, S. Paris, O. Chazot, and P. Omaly. Aerothermodynamics modelling of complex shapes in the DEBRISK atmospheric reentry tool: methodology and validation. In *70th International Astronautical Congress*, October 2019.